Thermal Behavior of Laminar Flow of Supercritical CO$_2$ in a Long Vertical Mini-Pipe under Constant and Stepped Wall Heat Flux

Mahdi Mohseni [*]

Department of Mechanical Engineering, Qom University of Technology, Qom 37181 46645, Iran

ABSTRACT

In this study, the convective heat transfer of supercritical carbon dioxide in a long vertical mini-pipe has been investigated numerically. The numerical solution has been performed with the finite volume method and by developing a CFD code. The pipe has a length of 5.5 m and a diameter of 1 mm which is exposed to a constant heat flux at the wall with values of 300, 400, 500, and 600 W/m^2 or step changes. In addition to the wall heat flux, the effects of gravity and flow direction have also been examined. Furthermore, some differences between the results of laminar and turbulent flows have been addressed. The results show that in the laminar flow, unlike the turbulent flow in the improvement regime of heat transfer, the system's thermal performance increases with increasing the wall heat flux, while in the deterioration mode, the two have similar behavior. Moreover, in part of the downward flow, reverse flow occurs, and its length can be understood by using the negative amount of wall shear stress. Furthermore, the thermal efficiency of the supercritical carbon dioxide is better at the upward flow and near the critical point than the constant property flow. In addition, from the applied stepped wall heat flux, it is concluded that the deterioration can be partially controlled or reduced by correctly determining the location of the step or any wall heat flux variations.

1. Introduction

Increasing thermal efficiency and changing some other properties of supercritical fluids, such as solubility, have led to using these fluids in many engineering systems in recent decades [1,2]. For example, the use of supercritical fluid in heat exchangers can be mentioned [3,4]. These heat exchangers are used in various industries, including extraction units or air conditioning systems of automobiles or power plants [5,6]. The design and performance of such heat exchangers have been the topic of ongoing research for many years [7,8].

Due to the complexity of supercritical fluid flow behavior and its increasing use, many studies have been conducted to investigate the thermal behavior and flow structure in this fluid. However, most of the research is related to turbulent flow, and the laminar flow has received less attention [9,10,11]. This may be because most industrial flows are turbulent, especially for normal or large pipe diameters. However, when the pipe diameter is too small, e.g., mini channels and microchannels [12,13,14], or the flow is in an annulus with a very small clearance, such as bearing [15], or the pipe contains porous material [16], the Reynolds number will naturally be small, and the flow will be in the laminar regime. Previous studies on laminar flow have investigated the effect of one or more important factors on supercritical fluid [17,18]. These factors mainly include wall heat flux, mass flux or Reynolds number, pipe diameter, and fluid type [18,19]. In some cases, the effect of channel cross-sections has been

[*]*Corresponding Author: Mahdi Mohseni*
Email: m.mohseni@qut.ac.ir

examined [20]. It should be noted that almost all research on laminar flow has been performed numerically. This may be because testing with supercritical conditions in laminar flows is impossible due to pressure and temperature fluctuations. Some of the research has been reviewed in more detail in the following.

In 2010, convection heat transfer of water at supercritical pressure in a narrow annulus was numerically investigated by Hassan Zaim and Gandjalikhan Nassab [21]. Their study showed that the effect of strong buoyancy force increases velocity near the wall. As a result, the convective heat transfer enhances. In 2011, Cao et al. [20] numerically investigated the laminar convection heat transfer of supercritical carbon dioxide in horizontal circular and triangular tubes with hydraulic diameters less than 1.0 mm. It was shown that due to the strong buoyancy force, secondary flows were created in the pipe cross-sections, which led to the distortion of the velocity and temperature profiles. Based on the analytical and numerical study of Peeters and T'Joen [22] in 2013, the thermally developing length in the upward flow of supercritical CO_2 and supercritical H_2O can be written as a function of a non-dimensional ratio of wall heat flux and Peclet number for the specific conditions that were used. Gao et al. [23] numerically investigated the effect of flow reversal at the entry length of a vertical annulus in laminar mixed convection flow of supercritical carbon dioxide in 2018. According to their results, the dominant effect of free convection is essential for flow reversal. Viswanathan and Krishnamoorthy [18], in 2021, conducted a series of numerical tests using Ansys-Fluent software to investigate the effect of heat flux, tube diameter, and inlet Reynolds number in a small diameter horizontal tube. According to their results, depending on the heat flux's magnitude and the fluid temperature's proximity to the critical point, the Nusselt number finds a value lower or higher than 4.36, corresponding to flows of constant properties. Finally, they introduced a relation for the Nusselt number.

Considering the widespread use of mini and microchannels as well as porous media in recent years, the laminar flow of supercritical fluid can be the subject of further research. Therefore, in this study, the effect of flow direction, gravity, and wall heat flux on wall temperature, heat transfer, and flow structure in the flow of supercritical carbon dioxide has been investigated by developing an axisymmetric CFD code. The studied geometry is a vertical mini-tube exposed to constant and stepped heat fluxes in the wall. To create more realistic conditions and cover the entire region near the pseudo-critical point, the length of the pipe is considered long. In addition, some differences between the laminar and turbulent flow of supercritical fluids have been noted.

2. Flow Description

In supercritical fluid flow, the changes in the fluid's thermo-physical properties are very intense near its critical points. Such changes in the fluid properties significantly affect flow structure and heat transfer [24,25]. As a sample, the changes in the properties of supercritical carbon dioxide at a pressure of 8 MPa are shown in Fig. 1. As the critical point approaches, the change in fluid properties becomes more severe.
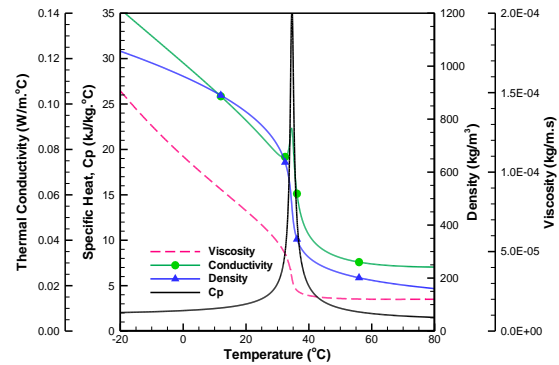

Figure 1. Variations of thermo-physical Properties of supercritical CO_2 at 8 MPa [26]

The problem under study is the flow of supercritical CO_2 inside a long vertical mini-pipe with a length of 5.5 m and a diameter of 1 mm. The flow can enter from the top or bottom of the pipe and exit from the other side. The schematic of the pipe is shown in Fig. 2. The first 20 cm and the last 30 cm of the pipe are insulated, and the rest of the pipe length is exposed to a constant heat flux of 300, 400, 500, and 600 W/m^2 or a step changes. Supercritical carbon dioxide enters the pipe at a pressure of 8 MPa, a mass flux of 40 $kg/s.m^2$, and a temperature of 27 °C (300 K). According to the mentioned conditions, the fluid flow is in the laminar regime.
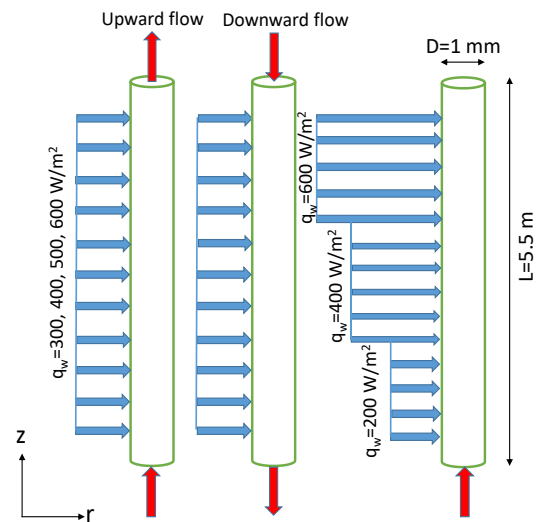

Figure 2. Schematic of the geometry under consideration

3. Governing Equations

According to the studied flow described in the previous section, the governing equations include the mass conservation equation, the momentum equation, and the energy equation which for the variable property flow of supercritical fluid in the steady state are as follows [27]. It should be noted that due to axisymmetric flow, the equations are written in a two-dimensional cylindrical coordinate system.

The mass conservation equation

$$\frac{1}{r}\frac{\partial}{\partial r}(r\rho v) + \frac{\partial}{\partial z}(\rho u) = 0 \tag{1}$$

The r-momentum equation

$$\frac{1}{r}\frac{\partial}{\partial r}(r\rho vv) + \frac{\partial}{\partial z}(\rho vu) =$$
$$\rho g_r - \frac{\partial P}{\partial r} + \frac{\partial}{\partial z}\left[\mu\left(\frac{\partial u}{\partial r} + \frac{\partial v}{\partial z}\right)\right] + \tag{2}$$
$$2\frac{\partial}{\partial r}\left(\mu\frac{\partial v}{\partial r}\right) - \frac{2}{3}\frac{\partial}{\partial r}(\mu u_{k,k})$$

The z-momentum equation

$$\frac{1}{r}\frac{\partial}{\partial r}(r\rho uv) + \frac{\partial}{\partial z}(\rho uu) =$$
$$\rho g_z - \frac{\partial P}{\partial z} + \frac{\partial}{\partial r}\left[\mu\left(\frac{\partial u}{\partial r} + \frac{\partial v}{\partial z}\right)\right] + \tag{3}$$
$$2\frac{\partial}{\partial z}\left(\mu\frac{\partial u}{\partial z}\right) - \frac{2}{3}\frac{\partial}{\partial z}(\mu u_{k,k})$$

The energy equation

$$\frac{1}{r}\frac{\partial}{\partial r}(r\rho vH) + \frac{\partial}{\partial z}(\rho uH) =$$
$$\frac{1}{r}\frac{\partial}{\partial r}\left(kr\frac{\partial T}{\partial r}\right) + \frac{\partial}{\partial z}\left(k\frac{\partial T}{\partial z}\right) + \frac{DP}{dt} \tag{4}$$
$$+ \dot{Q} + \varphi$$

where the dissipation function is defined as

$$\varphi = \mu\left[2\left\{\left(\frac{\partial v}{\partial r}\right)^2 + \left(\frac{v}{r}\right)^2 + \left(\frac{\partial u}{\partial z}\right)^2\right\}\right.$$
$$+ \left(\frac{\partial v}{\partial z} + \frac{\partial u}{\partial r}\right)^2 \tag{5}$$
$$\left. - \frac{2}{3}(\boldsymbol{\nabla} \cdot \boldsymbol{V})^2\right]$$

The definitions of the variables can be found in the nomenclature. To calculate the convection heat transfer coefficient, the following Newton cooling law is used.

$$h = \frac{q_w}{T_w - T_b} \tag{6}$$

Also, the local Nusselt number is defined as follows.

$$Nu = \frac{h\mathrm{D}}{\mathrm{k_f}} = \frac{qD}{\mathrm{k_f}[T_w - T_b(z)]} \tag{7}$$

The bulk enthalpy in each pipe cross-section is calculated from Eq. 8.

$$H_b = \frac{1}{GA}\int_0^R \rho vHdA = \frac{1}{GR^2}\int_0^R \rho vHrdr \tag{8}$$

The property database can also be used to obtain the bulk temperature corresponding to the bulk enthalpy.

4. Method of Solution

In order to discretize the governing equations, the finite volume method is used. The SIMPLE algorithm is applied along with the staggered grid to solve the velocity and pressure coupling equations. The hybrid scheme is also used to approximate the convective terms in the equations. This scheme is based on the intermittent use of central and upwind schemes and has high stability while physically producing realistic solutions [28]. The stability of the hybrid scheme becomes more apparent when, like the present study, the aim is to model the supercritical fluid flow. This is because, to model the high-variable property flow of supercritical fluids, the numerical solution tends to diverge. The SIMPLE algorithm and the hybrid scheme applied in the present CFD code are described extensively by Versteeg and Malalasekera [28].

To reach grid independency for the results, the solutions were obtained for various numbers of nodes in the radial and axial directions. Finally, 50 and 2200 grids were used in the radial and axial directions, respectively, so increasing the number of grids does not improve the results any further.

The significant property variations of supercritical fluids cause the governing equations to become highly coupled. In these conditions, the proper choice of under-relaxation factors (URFs) is essential to the convergence of the solution. Generally, the smaller values of URFs are needed compared to the constant property flows. The suitable URFs obtain by trial and error. The following convergence criterion for termination of calculations is used to ensure that the final answers are independent of the URFs.

$$R^\varphi < 10^{-5} \tag{9}$$

where

$$R^\varphi = \frac{\sum_{cell\ p}\left|\sum_{nb}a_{nb}\varphi_{nb} - b - a_p\varphi_p\right|}{\sum_{cell\ p}|a_p\varphi_p|} \tag{10}$$

5. Validation of the CFD Code

Due to the lack of experimental data for laminar flow, this section uses analytical solutions for the flow

with constant properties to validate the numerical simulation. For this purpose, the flow of water at a pressure of 1 atm in a pipe with 1.2 m length and 1 mm diameter is considered to validate the numerical results. Other flow conditions are listed in Table 1.

Table 1. Flow conditions were used for the validation of the CFD code.

Property	Value	Unit
Inlet velocity	0.05	m/s
Inlet temperature	20	^{o}C
Wall heat flux	1000	W
Density	1000	Kg/m^3
Viscosity	0.001	Kg/m.s
Specific heat capacity	4182	J/kg.^{o}C
Thermal conductivity	0.6	W/m.^{o}C

Figure 3 shows the value of the Nusselt number. As can be seen in the developed flow section, the value of the Nu is exactly 4.36, which entirely agrees with the analytical solution [29]. It should be noted that similar to the flow conditions for supercritical fluid in the next section, the beginning of the pipe is insulated, and heat transfer starts from a distance of 20 cm.
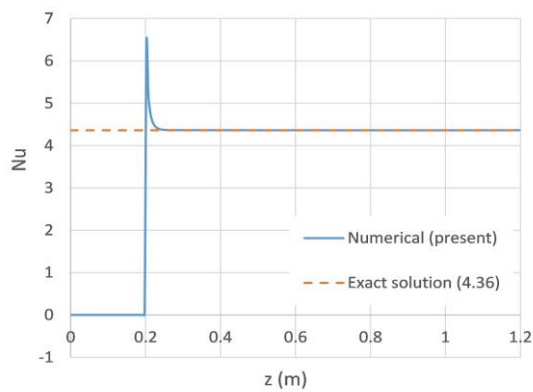

Figure 3. Variations of Nusselt number along the pipe for water at a pressure of 1 atm

Numerical results for bulk temperature are also compared with the analytical values in Fig. 4. The fluid's analytical bulk temperature in each pipe cross-section can be obtained from the energy balance along the pipe. Due to the imposition of constant heat flux in the pipe wall, it can be written:

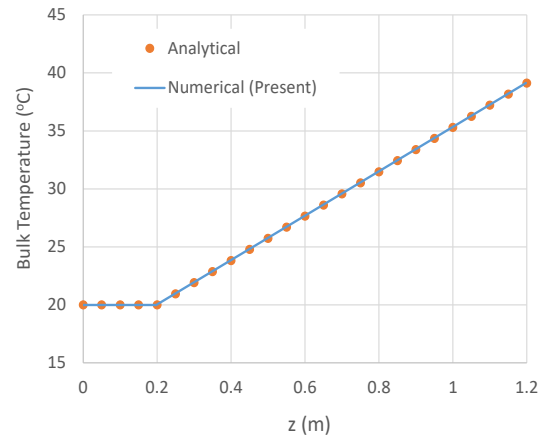$$T_b(x) = T_i + \frac{q\pi D}{\dot{m}C_p}x \qquad (11)$$

Figure 4. Variations of bulk temperature along the pipe for water at a pressure of 1 atm

It is observed from Fig. 4 that the two temperatures agree with each other. In addition, validating the present code for the turbulent flow of supercritical fluid has already been performed [30, 31].

6. Results and Discussion

This section investigates the effects of various factors affecting the system's thermal performance, which is explained in section 2. The results are divided into three parts as follows.

6.1. Effect of Flow Direction and Gravity

In supercritical conditions, drastic changes in fluid density produce strong buoyancy force as well as flow acceleration near the wall [32]. This leads to wall temperature and velocity profile changes compared to normal flows. Figures 5 to 7 show the velocity profiles at different pipe sections for the three situations studied in this study, i.e., upward, downward, and no-gravity flows for the wall heat flux of 300 W/m^2.
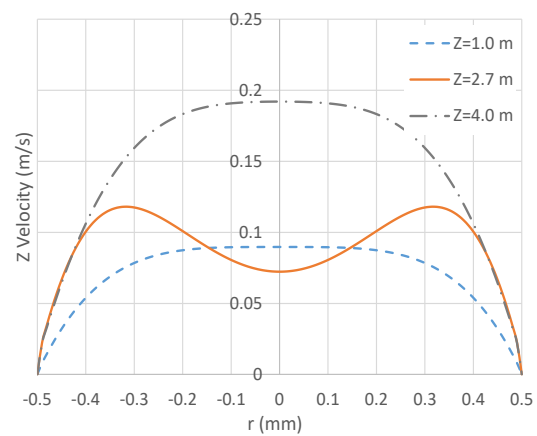

Figure 5. Velocity profiles for three cross-sections of the pipe in upward flow.
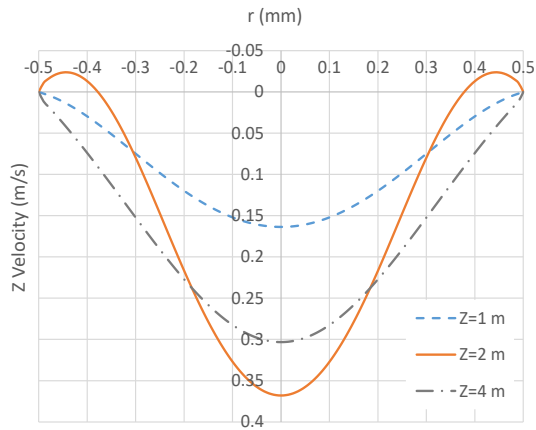
Figure 6. Velocity profiles for three cross-sections of the pipe in the downward flow.
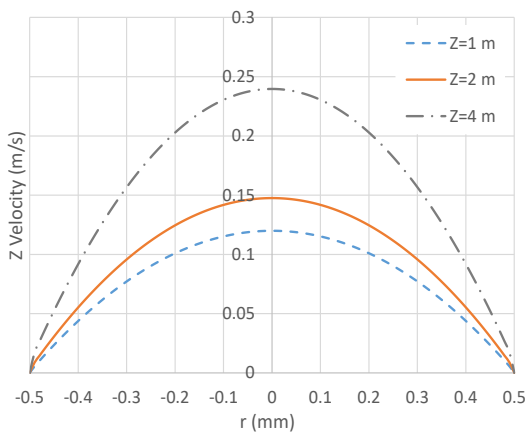

Figure 7. Velocity profiles for three cross-sections of the pipe in the no-gravity flow.

As can be seen from these figures, in the upward flow, the velocity profile deviates from the parabolic state in parts of the pipe and becomes like the letter M.

In other words, the maximum fluid velocity does not occur in the center of the pipe, but its location will be near the pipe wall. In the downward flow, the buoyancy force also causes the flow to return near the wall, forming a swirling flow in this region. None of these effects exist in the no-gravity flow without buoyancy force.

In addition, Fig. 7 shows that the velocity continuously increases as it moves downstream of the pipe, similar to the flow in a nozzle. This is due to the decrease in the density of the supercritical fluid.

For this reason, in supercritical fluid flows, unlike normal flows, the Reynolds number is not constant and increases significantly along the length of the pipe. The flow may become turbulent if the pipe length is long enough or the inlet flow velocity is high enough.

Fig. 8 shows the changes in average velocity and Reynolds number for the conditions of the present problem.
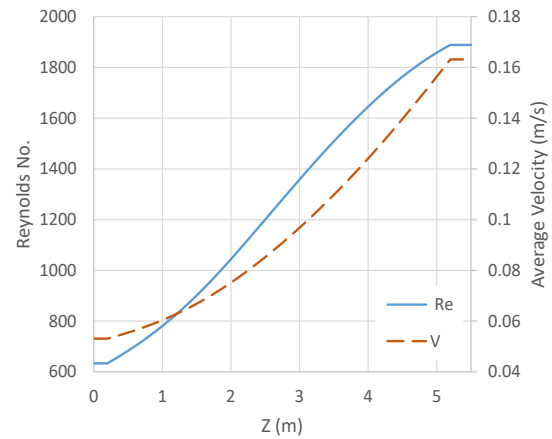

Figure 8. Variations of average velocity and Reynolds number along the pipe for q_w=300 W/m^2.

The shear stress direction is reversed in the region where the flow returns near the wall, and its value becomes negative. Fig. 9 shows the changes in the wall shear stress for the three investigated cases. As can be seen, only in the downward flow in a part of the pipe the amount of shear stress is negative, which indicates the return of the flow in this area. Depending on the applied heat flux and the inlet flow conditions, this region shifts or disappears altogether.
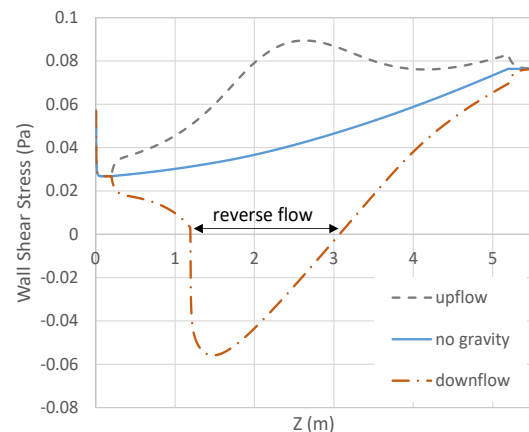

Figure 9. Variations of wall shear stress along the pipe for upward, downward and no-gravity flows for q_w=300 W/m^2.

When the buoyancy force is strong (for example, when the applied wall heat flux is large compared to the mass flux), one of the phenomena that may occur in supercritical fluid flow is heat transfer deterioration [24,25,32]. Because of the deterioration, the wall temperature increases suddenly, leading to an unsafe system in some conditions. To see this issue, the longitudinal changes of the wall temperature for three cases of this study are shown in Fig. 10. It should be noted that the deterioration occurs when the fluid temperature near the wall reaches the pseudo-critical value at high heat fluxes [29]. This phenomenon is also the reason for the sudden decrease in wall shear stress at z=1.2 m in Fig. 9 for downward flow.

It can be seen from Fig. 10 that very little deterioration occurred, only for the downward flow. On the other hand, increasing the wall temperature means reducing the heat transfer coefficient.

For the three cases examined in this study, the changes in the heat transfer coefficients are shown in Fig. 11. It is observed that when the wall temperature is suddenly increased, the heat transfer coefficient decreases drastically. The highest heat transfer coefficient is related to the upward flow. It should be noted that the reason for the zero heat transfer coefficient at the beginning and end of the pipe is the zero heat flux in these parts, that is, the insulation of the pipe in these sections. It is interesting to note that in the turbulent flow of supercritical fluid, this phenomenon occurs in the upward flow [31,33]. This is because the co-direction of flow and buoyancy force usually leads to a decrease in the flow turbulence and, thus, a decrease in the heat transfer coefficient. When turbulent flow is downward, the interaction of the buoyancy force and the flow direction increases the heat transfer.
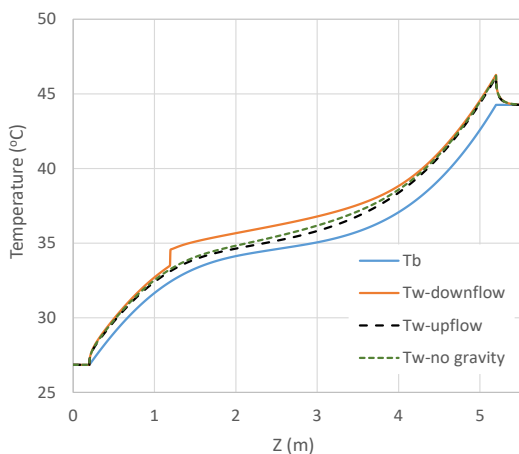

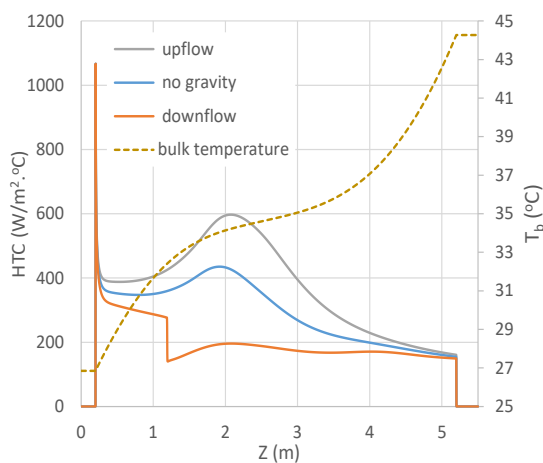**Figure 10.** Effect of flow direction and gravity on wall temperature variations for q_w=300 W/m².

Figure 11. Effect of flow direction and gravity on variations of heat transfer coefficients (HTC) for q_w=300 W/m².

One parameter that shows a heating system's performance is the Nusselt number. For this reason, Fig. 12 shows the changes in this parameter for the three studied cases. The analytical value of 4.36, corresponding to constant property flows, is also plotted for comparison. As can be seen, in the upward flow throughout the pipe and the no-gravity flow, only in parts of the pipe, the value of the Nusselt number is greater than 4.36. In other words, Fig. 12 shows that the system's thermal performance is unsuitable in the downstream flow.

In supercritical conditions similar to subcritical conditions, the buoyancy effect is usually expressed in terms of the dimensionless Grashof and Reynolds numbers as follows [34,35].
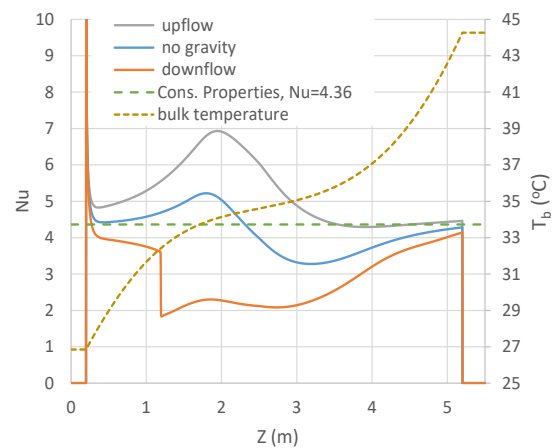
$$B = \frac{Gr_b}{Re_b^n} \qquad (12)$$

Figure 12. Effect of flow direction on Nu number for q_w= 300 W/m² and comparison with constant property flow conditions (Nu=4.36)

Where both b in both Gr_b and Re_b is subscript are defined based on bulk properties. The value of n is equal to 2 and 2.7 according to the results of Shiralkar and Griffith [34] and Johnson and Hall [35], respectively. Based on the criterion of Shiralkar and Griffith [34], if B>0.01, the effect of buoyancy is important and should be considered in the calculations, while according to the criterion of Johnson and Hall [35], B should be greater than 10^{-5} to consider buoyancy effect. In Fig. 13, the changes of parameter B are plotted for both upstream and downstream flows. It is seen that for both directions and based on both criteria, the effect of buoyancy is important throughout the pipe length and cannot be ignored. Moreover, the value of B is much higher for downward flow than upward flow.

2.2. Effect of Different Constant Wall Heat Flux

Based on previous results for turbulent flow in the literature, increasing the wall heat flux in both upward and downward flows has a negative effect on the

magnitude of the Nusselt number or heat transfer coefficient [31,33]. In this section, this issue is investigated for laminar flow. To do this, several simulations are performed for different wall heat fluxes from 300 to 600 W/m². The obtained results for the Nusselt number in the upward flow, the wall temperature, and the wall shear stress in the downward flow are plotted in Figures 14 to 16, respectively.
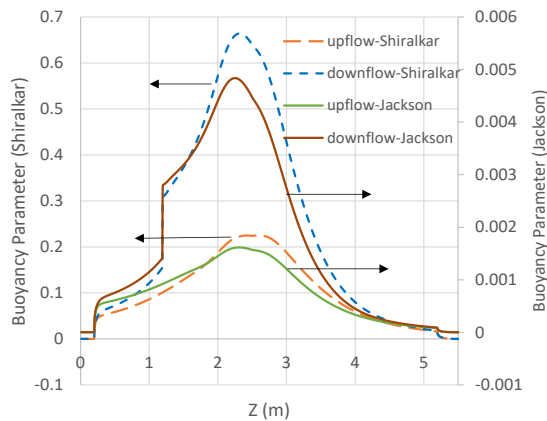

Figure 13. Variations of buoyancy parameters for upward and downward flows based on two criteria of Shiralkar [34] and Jackson [35] for q_w= 300 W/m².
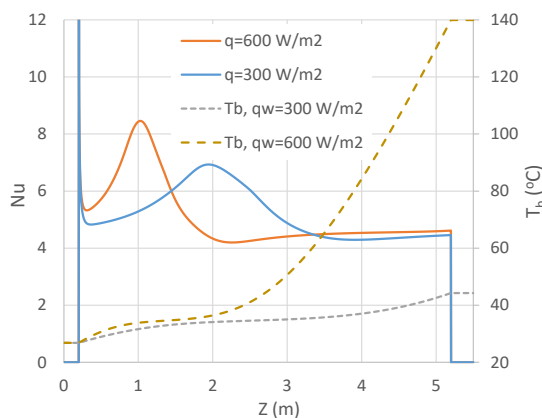

Figure 14. Effect of wall heat flux on axial variations of Nu number in upward flow.
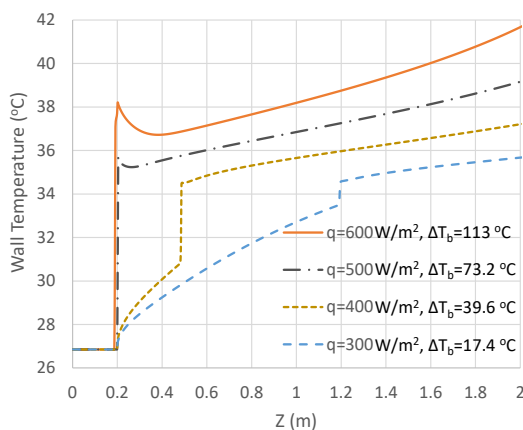

Figure 15. Effect of wall heat flux on axial variations of wall temperature in the downward flow.
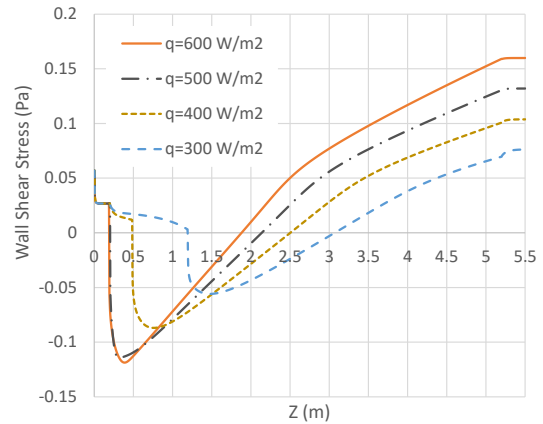

Figure 16. Effect of wall heat flux on axial variations of wall shear stress in the downward flow

It can be found from Fig. 14 that in laminar flow, as opposed to turbulent flow with increasing the wall heat flux in the improvement regime, the Nusselt number increases. However, similar to turbulent flow, as shown in Fig. 15 when deterioration occurs, increasing heat flux leads to a further increase in wall temperature, which means a further reduction of Nusselt number in this area. It should be noted that, as mentioned earlier, regimes of improvement and deterioration of heat transfer in a vertical tube in the laminar flow are opposite to the turbulent flow. It can also be seen from Fig. 15 that with increasing the wall heat flux, the sudden increase in wall temperature is approaching the pipe inlet and in heat fluxes of 500 and 600 W/m² due to the proximity of the inlet temperature to the pseudo-critical temperature, this phenomenon appears as soon as the heat flux is applied. Similar behavior observes in Fig. 16 for the wall shear stress when the wall heat flux increases. In other words, at higher heat fluxes, the return flow begins at the inlet of the pipe at the same location where the heat flux is applied.

2.3. Effect of Stepped Wall Heat Flux

Because the heat flux of the wall may not be the same in all parts of the pipe where the heat transfer takes place, in this section, the effect of a step change of the wall flux on the thermal behavior of the system is investigated. The results for Nusselt number are shown in Fig. 17. It is seen that when the heat flux changes, the Nusselt number also jumps abruptly, resulting from the temperature difference at these points. Like the previous results, the Nusselt number for the upward flow near the critical point has higher values than the constant property flow. Under these conditions, the downward flow deteriorated. In fact, in the location where the second step of the wall heat flux is applied, i.e., at z=1.2 m, the wall temperature passes from the pseudo-critical temperature, which in turn causes deterioration to occur at this point. This phenomenon is shown in Fig. 18. It may be concluded

that the deterioration can be partially controlled or reduced by correctly determining the location of the step or any variation related to the wall heat flux. Deterioration, on the other hand, causes a sudden decrease in wall shear stress in downward flow, as shown in Fig. 19. In other words, the reverse flow starts in this region.
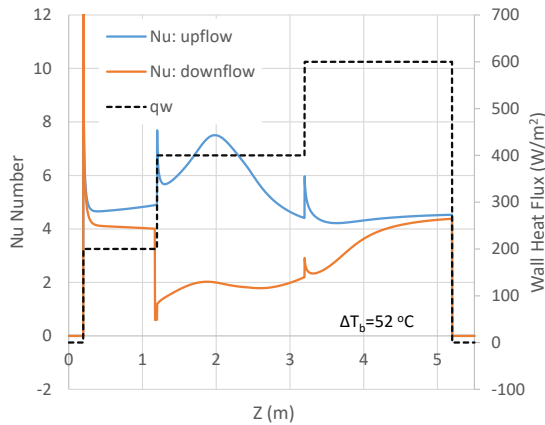

Figure 17. Effect of stepped wall heat flux on longitudinal variations of Nu number for both upward and downward flows.
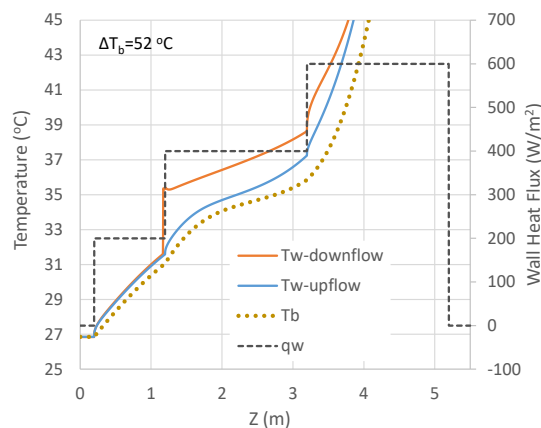

Figure 18. Effect of stepped wall heat flux on longitudinal variations of wall and bulk temperatures for both upward and downward flows.
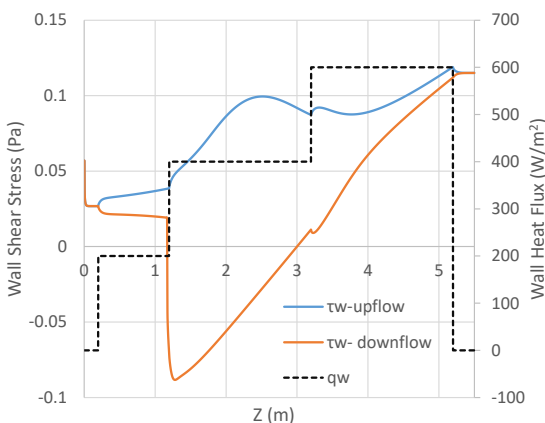

Figure 19. Effect of stepped wall heat flux on longitudinal variations of wall shear stress for both upward and downward flows.

7.   Conclusion

In this study, the laminar flow of supercritical CO_2 in a long vertical mini-pipe has been numerically investigated by developing an axisymmetric CFD code. The effect of some important parameters, including flow direction, constant and stepped wall heat flux, and gravity, are examined. Severe changes in fluid properties and gravity force produce strong buoyancy force, significantly affecting the flow's structure and thermal behavior. The following are the most important results of this study.

*   Unlike turbulent flow, buoyancy force causes the heat transfer coefficients in the laminar regime in the upward flow to be higher than the downward flow. In other words, the heat transfer deteriorates in the downward flow, accompanied by a sudden increase in the wall temperature. In addition, in the downward flow in the part of the pipe where the fluid is near the critical point, reverse flow occurs near the wall. In this area, the shear stress of the wall has a negative value from which the length of the reverse flow can be understood. When gravity is assumed to be absent, the thermal performance lies between the two.

*   It is observed that in the laminar flow, unlike the turbulent flow, in the improvement regime of heat transfer with increasing the wall heat flux, the maximum Nusselt number and heat transfer coefficient increase. In the deterioration regime, however, similar to turbulent flow, the jump in the wall temperature increases with increasing the wall heat flux.

*   It may be possible by correctly determining the location of the step or any other changes of the wall heat flux as much as possible, the deterioration partially controlled or reduced. This issue needs further research.

*   In the laminar flow of supercritical fluids, if the length of the pipe is long enough, the laminar flow may become turbulent, which is especially important in numerical modeling. In the present case, the Reynolds number goes from 630 at the pipe inlet to about 2005 at the pipe outlet.

Nomenclature

Cp	Specific heat capacity [J/kg.K]
d	Pipe diameter [m]
g	Gravitational acceleration [m/s^2]
G	Mass flux [kg/s.m^2]
h	Heat transfer coefficient [W/m^2.K]
H	Enthalpy [J/kg]
k_f	Thermal conductivity [W/m.K]

Nu   Nusselt number

p   Pressure [N/m^2]

q   Heat flux [W/m^2]

$\dot{Q}$ Internal Heat Source [W/m^3]

r   Radial direction of flow [m]

Re   Reynolds number [$Re=\rho VD/\mu$]

T   Temperature [^oC]

u   Velocity component in z direction [m/s]

v   Velocity component in r direction [m/s]

z   Axial direction of flow [m]

Greek Symbols

ϕ   Dissipation function in energy equation $kg/m.s^3$

μ   Molecular viscosity [kg/m.s]

ρ   Density [kg/m^3]

τ   Shear stress [N/m^2]

Subscript

b   Bulk

i   Inlet

w   Wall

Conflicts of Interest

The author declares that there is no conflict of interest regarding the publication of this manuscript. In addition, the authors have entirely observed the ethical issues, including plagiarism, informed consent, misconduct, data fabrication and/or falsification, double publication and/or submission, and redundancy.

References

[1] Yamaguchi, H. et al., 2010. Preliminary Study on a Solar Water Heater Using Supercritical Carbon Dioxide as Working Fluid. Journal of Solar Energy Engineering, 132(1), p.011010.

[2] Pecnik, R., Rinaldi, E., and Colonna, P., 2012. Computational fluid dynamics of a radial compressor operating with supercritical CO_2. ASME Journal of Engineering Gas Turbines Power, 134 (12), p.122301.

[3] Serrano, I.P. et al., 2014. Modeling and sizing of the heat exchangers of a new supercritical CO_2 Brayton power cycle for energy conversion for fusion reactors. Fusion Engineering and Design, 89(9), pp.1905–1908.

[4] Gkountas, A.A. et al., 2020. Heat transfer improvement by an Al_2O_3-water nanofluid coolant in printed-circuit heat exchangers of supercritical CO_2 Brayton cycle. Thermal Science and Engineering Progress, 20, p.100694.

[5] Lee, Y., and Lee, J.I. 2014. Structural assessment of intermediate printed circuit heat exchanger for sodium-cooled fast reactor with supercritical CO_2 cycle, Annual Nuclear Energy, 73, pp.84–95.

[6] Besarati, S. M., Goswami, D. Y., and Stefanakos, E. K., 2015. Development of a solar receiver based on compact heat exchanger technology for supercritical carbon dioxide power cycles. ASME Journal of Solar Energy Engineering, 137(3) p.031018.

[7] Jin, K., Krishna, A.B., Wong, Z., Ayyaswamy, P.S., Catton, I., and Fisher, T.S., 2023. Thermohydraulic experiments on a supercritical carbon dioxide–air microtube heat exchanger. International Journal of Heat and Mass Transfer, 203, p.123840.

[8] Krishna, A.B., Jin, K., Ayyaswamy, P.S., Catton, I., and Fisher, T.S., 2023. Technoeconomic optimization of superalloy supercritical CO_2 microtube shell-and-tube-heat exchangers. Applied Thermal Engineering, 220, p.119578.

[9] Simoneau, R.J. and Williams, J.C., 1969. Laminar couette flow with heat transfer near the thermodynamic critical point. International Journal of Heat and Mass Transfer, 12, pp.120-124.

[10] Kim, J.K., and Aihara, T., 1992. A numerical study of heat transfer due to an axisymmetric laminar impinging jet of supercritical carbon dioxide. International Journal of Heat and Mass Transfer, 35 (10), pp.2515-2526.

[11] Lee, S.H. and Howel, J.R., 1996. Laminar forced convection at zero gravity to water near the critical region. Journal of Thermophysics and heat transfer, 10 (3), p.504.

[12] Liao, S.M. and Zhao, T.S., 2002. A numerical investigation of laminar convection of supercritical carbon dioxide in vertical mini/micro tubes. Progress in Computational Fluid Dynamics, 2 (2/3/4) pp.144–152.

[13] Khalesia, J., Sarunac, N. and Razzaghpanaha, Z., 2020. Supercritical CO_2 conjugate heat transfer and flow analysis in a rectangular microchannel subject to uniformly heated substrate wall. Thermal Science and Engineering Progress, 19, p.100596.

[14] Saeed, M. Berrouk, A.S. AlShehhi, M.S. and AlWahedi, Y.F., 2021. Numerical investigation of the thermohydraulic characteristics of microchannel heat sinks using supercritical CO_2 as a coolant. The Journal of Supercritical Fluids, 176, p. 105306.

[15] Rafee, R., 2014. Entropy generation calculation for laminar fully developed forced flow and heat transfer of nanofluids inside annuli, Journal of Heat and Mass Transfer Research, 1(1), pp. 25–33.

[16] Zolfaghar, M. and Mohseni, M., 2021. Numerical study of the effect of hole arrangement on thermal efficiency of a pipe containing perforated porous media. Thermal Science Engineering Progress, 25, p.100999.

[17] Dang C., and Hihara E., 2010. Numerical study on in-tube laminar heat transfer of supercritical fluids. Applied Thermal Engineering, 30, pp.1567-1573.

[18] Viswanathan, K. and Krishnamoorthy, G., 2021. The effects of wall heat fluxes and tube diameters on laminar heat transfer rates to supercritical CO_2. International Communications in Heat and Mass Transfer, 123, p.105197.

[19] Zhang, X.R. and Yamaguchi, H., 2007. Forced convection heat transfer of supercritical CO_2 in a horizontal circular tube. Journal of Supercritical Fluids, 41, pp.412–420.

[20] Cao, X.L., Rao, Z.H., Liao, S.M., 2011. Laminar convective heat transfer of supercritical CO_2 in horizontal miniature circular and triangular tubes. Applied Thermal Engineering, 31, pp.2374-2384.

[21] Hassan Zaim, E., and Gandjalikhan Nassab, S.A., 2010. Numerical investigation of laminar forced convection of water upwards in a narrow annulus at supercritical pressure. Energy 35, pp.4172-4177.

[22] Peeters, J.W.R., T'Joen, C. and Rohde, M., 2013. Investigation of the thermal development length in annular upward heated laminar supercritical fluid flows. International Journal of Heat and Mass Transfer, 61, pp.667–674.

[23] Gao, W., Abdi-khanghah, M., Ghoroqi, M., Daryasafar, A., and Lavasani, M., 2018. Flow reversal of laminar mixed convection for supercritical CO_2 flowing vertically upward in the entry region of asymmetrically heated annular channel. The Journal of Supercritical Fluids, 131, pp.87-98.

[24] Mohseni, M., and Bazargan, M., 2012. A new analysis of heat transfer deterioration on basis of turbulent viscosity variations of supercritical fluids. Journal of Heat Transfer, T-ASME, 134 (12), p.122503.

[25] Mohseni, M., and Bazargan, M., 2012. New analysis of heat transfer deterioration based on

supercritical fluid property variations. Journal of Thermophysics and Heat Transfer, 26, pp.197-200.

[26] Lemmon, E., Huber, M. and McLinden, M., 2013. NIST Standard Reference Database 23: Reference Fluid Thermodynamic and Transport Properties-REFPROP, Version 9.1, Natl Std. Ref. Data Series (NIST NSRDS), National Institute of Standards and Technology, Gaithersburg, MD, [online], https://tsapps.nist.gov/publication/get_pdf.cfm?pub_id=912382

[27] Bird, R.B., Stewart, W.E., Lightfoot, E.N., Klingenberg, D.J., 2015. Introductory Transport Phenomena. John Wiley & Sons, Inc, USA.

[28] Versteeg, H.K., and Malalasekera, W., 2007. An Introduction to Computational Fluid Dynamic, The Finite Volume Method. 2nd ed., Pearson Education Limited, London, UK.

[29] Cengel, Y.A., Cimbala, J.M., Turn, R.H., 2017. Fundamentals of thermal-fluid sciences. 5th edition, McGraw Hill Education, New York, USA.

[30] Bazargan, M. and Mohseni, M., 2009. The significance of the buffer zone of boundary layer on convective heat transfer to a vertical turbulent flow of a supercritical fluid. The Journal of Supercritical Fluids, 51, pp.221-229.

[31] Mohseni, M., and Bazargan, M., 2011. The effect of the low Reynolds number k-e turbulence models on simulation of the enhanced and deteriorated convective heat transfer to the supercritical fluid flows. Heat and Mass Transfer, 47, pp.609–619.

[32] Kumar, D.S, Suresh S., and Sundaravel, A., 2019. Heat Transfer Studies of Supercritical Water Flows in an Upward Vertical Tube. Journal of Heat and Mass Transfer Research, 6(2), pp.155–167.

[33] Yamagata, K., Nishikawa, K., Hasegawa, S., Fuji, T., and Yoshida, S., 1972. Forced convective heat transfer to supercritical water flowing in tubes. International Journal of Heat and Mass Transfer, 15 (12), pp.2575-2593.

[34] Shiralkar B.S., Griffith P., 1970. The effect of swirl, inlet condition, flow direction and tube diameter on heat transfer to fluids at supercritical pressure. ASME J. Heat Transfer, 92, pp.465-474.

[35] Jackson, J.D., Cotton, M.A., and Axcell, B.P., 1989. Studies of mixed convection in vertical tubes. International Journal of Heat and Fluid Flow, 10 (1), pp.2-15.